Anomalous thermoelectric effects and quantum oscillations in the kagome metal CsV$_3$Sb$_5$

Dong Chen [1,2,*] Bin He,[1] Mengyu Yao,[1] Yu Pan,[1] Haicheng Lin,[1] Walter Schnelle,[1] Yan Sun,[1]
Johannes Gooth,[1] Louis Taillefer,[3,4] and Claudia Felser[1,4,†]

[1]*Max Planck Institute for Chemical Physics of Solids, 01187 Dresden, Germany*
[2]*College of Physics, Qingdao University, Qingdao 266071, China*
[3]*Institut Quantique, Département de Physique and RQMP, Université de Sherbrooke, Sherbrooke, Québec, Canada*
[4]*Canadian Institute for Advanced Research, Toronto, Ontario, Canada*

The kagome metal compounds AV$_3$Sb$_5$ ($A =$ K, Rb, and Cs) feature a wealth of phenomena including nontrivial band topology, charge density wave (CDW), and superconductivity. One intriguing property is the time-reversal symmetry breaking in the CDW state without local moments, which leads to anomalous transport responses. Here, we report the investigation of magnetothermoelectric effects on high-quality CsV$_3$Sb$_5$ single crystals. A large anomalous Nernst effect (ANE) is observed at temperatures below 30 K and can be enhanced by the high mobility. Multiple Fermi surfaces with small effective masses are revealed by quantum oscillations in the Nernst and Seebeck signals. Furthermore, we discover a magnetic breakdown effect across the two smallest Fermi surfaces, with a gap around 20 meV between them. We propose that the two Fermi surfaces are split from a Dirac band by the CDW gap. These results indicate the large ANE originates from the CDW modulated nontrivial band structure as well as the extrinsic contributions. A second phase transition below the CDW transition temperature is also suggested by the strange temperature dependence of the ANE.

Condensed matter systems with kagome lattices have attracted significant interest owing to their rich physics. With the special two-dimensional corner-sharing triangular network, the electronic structure of the kagome lattice holds Dirac cones, flat bands, and enhanced correlation [1,2]. Further inclusion of other collective orders in metallic kagome materials can give rise to more exotic quantum states and phenomena [3–10]. Recently, a new kagome metal family AV$_3$Sb$_5$ ($A =$ K, Rb, and Cs) was discovered, hosting a superconducting ground state with the critical temperature (T_c) ranging from 0.93 K for KV$_3$Sb$_5$ to 2.5 K for CsV$_3$Sb$_5$, as well as a charge-density-wave (CDW) transition at $T_{CDW} = 80$, 103, and 94 K, respectively [11–14]. Band-structure calculations revealed multiple van Hove singularities, Dirac cones, and the nontrivial $\mathbb{Z}_2$ topology [14,15]. The unusual band structure modulated by CDW is relevant for various interesting properties, such as unconventional superconductivity, chiral charge order, and time-reversal symmetry breaking (TRSB) without local moments [14–24].

Generally, in a band structure with Dirac cones close to the Fermi level, the TRSB can open an energy gap at the Dirac points, thereby generating a large Berry curvature [25]. The Berry curvature acts as a magnetic field in the momentum space, and leads to the anomalous Hall effect (AHE) and anomalous Nernst effect (ANE), even without ferromagnetism [26]. According to the Mott relation, the thermoelectric effects are proportional to the energy derivative of the electric conductivities at the Fermi level [27]. The thermoelectric effects are more sensitive to the Berry curvature near the Fermi level than the respective electric conductivities. The large ANE induced by the Berry curvature has been observed in Cd$_3$As$_2$ and ZrTe$_5$ [28,29]. Furthermore, the quantum oscillations in the thermoelectric coefficients are typically stronger compared to the Shubnikov–de Haas (SdH) oscillations, which can provide relevant information on the band structure [30].

In this Letter, we report a study of magnetothermoelectric properties in high-quality single crystals of CsV$_3$Sb$_5$. We observe large ANE below a temperature of 30 K that is enhanced by high mobility. The Seebeck coefficient shows a mustache shape in low field, as a consequence of the multiband effect. Significant quantum oscillations are present in both Seebeck and Nernst signals, revealing a magnetic breakdown across the two smallest Fermi surfaces (FSs). We argue that these two small FSs are split from a single Dirac band by the CDW gap. These results suggest both intrinsic and extrinsic contributions to the large ANE, provide more explicit information on the CDW modulated band structure, and reveal a second phase transition below T_{CDW} in this system.

High-quality single crystals of CsV$_3$Sb$_5$ were grown using the self-flux method [14]. The transport properties were measured in a Quantum Design physical properties measurement system. The Seebeck and Nernst signals were measured by a self-built one-heater–two-thermometers setup with $H \parallel c$ and $-\nabla T \parallel a$ crystallographic directions [31]. We report the
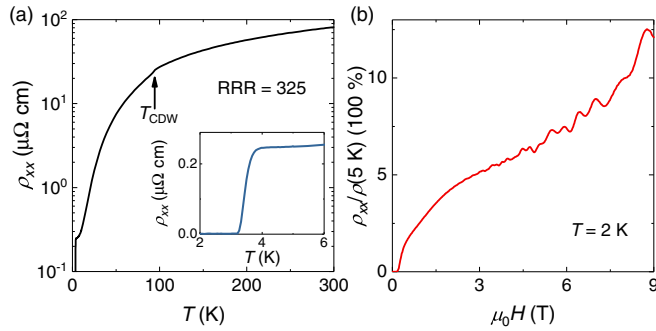
FIG. 1. (a) Temperature dependence of the resistivity of a typical sample with the RRR as high as 325. The kink at 94 K corresponds to the CDW transition. The inset shows the low-temperature resistivity with a sharp superconducting transition at 3.5 K. (b) Resistivity at 2 K divided by the normal-state resistivity $\rho(5\,\text{K})$ as a function of magnetic field. The high RRR and magnetoresistance, sharp superconducting transition, and intense quantum oscillations suggest the high quality of the samples.

thermoelectric results for two samples, #1 and #2. The temperature difference on sample #1 was measured with Cernox thermometers from 2 to 25 K, while on sample #2 it was determined with type-E thermocouples from 10 to 300 K.

Figure 1 shows the resistivity (ρ_{xx}) of a typical crystal as the functions of temperature and magnetic field. The resistivity displays a kink due to the CDW transition at 94 K, and a superconducting transition at 3.5 K. All the behaviors are similar to previous reports [14,21], except for the extremely large residual resistivity ratio RRR = $\rho(300\,\text{K})/\rho(5\,\text{K})$ of 325 [Fig. 1(a)]. Also, the sample shows a much larger magnetoresistance and evident SdH oscillations as shown in Fig. 1(b). The magnetoresistance at 2 K referenced to $\rho(5\,\text{K})$ exceeds 1000% at 9 T. All the results indicate a low defect density that guarantees the long mean free path of carriers in cryogenic temperatures. These features can provide the preferable condition for large ANE and magnetic breakdown, which are discussed in the following.

Figures 2(a) and 2(b) show the magnetic field dependence of the Nernst signal S_{xy}/T for samples #1 and #2 at selected temperatures, respectively. In the semiclassical one-band theory, the Nernst thermopower S_{xy} evolves with magnetic field as $S_{xy} = S_0 \mu B/[1 + (\mu B)^2]$, where μ is the carrier mobility. It has a peak at $B = 1/\mu$ and tends to zero under higher field [32]. The Nernst signal of both samples #1 and #2 shows a weak peak below 1 T, and the peak field value increases with temperature. The low peak field underlines the high mobility of the charge carriers. At low temperatures, the Nernst signals display intense quantum oscillations, and tend to a nonzero constant in the high-field region, which is an obvious anomalous component. As the temperature increases, the anomalous component gradually vanishes. At higher temperatures, a linear behavior with a negative slope becomes noticeable, which is caused by the multiband effect [33,34].

To further reveal the origin of the ANE, we extract the anomalous Nernst component by the linear extrapolation of $S_{xy}(B)$ to zero field, as shown in Fig. 2(c). Although the anomalous component for sample #1 is larger than that of sample #2, they have a similar temperature dependence in
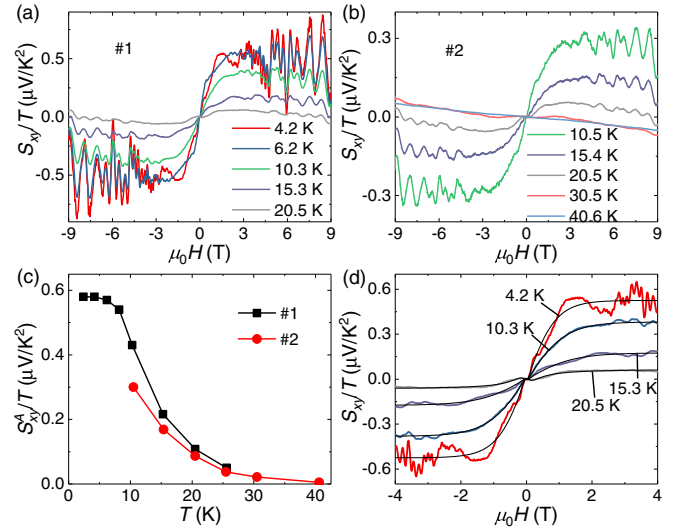
FIG. 2. (a), (b) Magnetic field dependence of the Nernst signal S_{xy}/T at various temperatures for samples #1 and #2, respectively. (c) Anomalous Nernst signals of the two samples as a function of temperature. (d) Fitting of the Nernst signal with the empirical expression (1) at selected temperatures. The black lines indicate the fitting curves.

the overlapping range. The ANE component has almost no temperature dependence at low temperatures, and rapidly decreases at higher temperatures until about 30 K. The low-field Nernst curves can also be described by an empirical expression [28],

$$S_{xy}(B) = S_{xy}^N \frac{\mu B}{1 + (\mu B)^2} + S_{xy}^A \tanh\left(\frac{B}{B_0}\right), \qquad (1)$$

where S_{xy}^N and S_{xy}^A are the ordinary and anomalous Nernst signal amplitudes, respectively. B_0 is the saturation field of the anomalous component. This expression fits well with the Nernst signals for low temperatures, and some examples of the fits are shown in Fig. 2(d). They result in a very high mobility of $\mu \sim 10^5\,\text{cm}^2\,\text{V}^{-1}\,\text{s}^{-1}$ for sample #1 and an order of magnitude lower for sample #2. The mobility difference can also be perceived by comparing the Nernst signals of the two samples at the same temperature, where the quantum oscillations of sample #1 are obviously greater than those of sample #2 [31]. These features suggest the enhancement effect of the mobility to the ANE.

Figures 3(a) and 3(b) show the Seebeck coefficient S_{xx} for both samples at selected temperatures. Also, the Seebeck signals of the two samples have a similar magnetic field dependence and close values. The temperature dependence of the zero-field S_{xx} for both samples is shown in Fig. 3(c). It is negative for $T > 6$ K, indicating the dominant electron carriers, but becomes positive for lower temperatures, proving the existence of two types of carriers. Moreover, for temperatures below $\sim$20 K the Seebeck signal has a mustache-shaped profile around zero field, which cannot be explained by the conventional one-band model [32]. Considering the multiband nature of the system, we use the
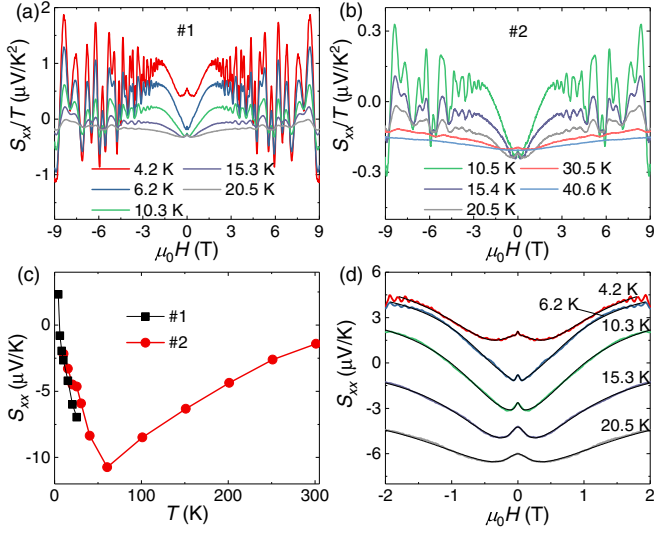
FIG. 3. (a), (b) Magnetic field dependence of the Seebeck signals for samples #1 and #2, respectively. (c) Temperature dependence of the Seebeck coefficient at zero field for both samples. (d) Seebeck signal of sample #1 with the fitting lines of the two-band expression (2).

modified expression [31]

$$S_{xx}(B) = S_1 \frac{1}{1 + (\mu_1 B)^2} + S_2 \frac{1}{1 + (\mu_2 B)^2} + S_\infty \frac{(\mu' B)^2}{1 + (\mu' B)^2},$$
(2)

where S_1 (S_2) and μ_1 (μ_2) are the zero-field Seebeck coefficients and mobility of the first (second) carrier, respectively, and S_∞ is the limiting value when $B \to \infty$. The expression can well fit the Seebeck signals, as shown in Fig. 3(d). The obtained mobilities of the carriers are in the same orders of magnitude with the values from Nernst signals, and are higher for sample #1 than those of sample #2.

The quantum oscillations can provide more information on the electronic structure. Figure 4(a) shows the oscillatory parts ΔS_{xx} and ΔS_{xy} at 2.4 K. Although composed of multiple frequencies, the oscillations have one primary frequency for both ΔS_{xx} and ΔS_{xy} as marked by the dashed lines. As shown in Fig. 4(b), the fast Fourier transformation (FFT) of ΔS_{xx} reveals four main frequencies, which are $F_\alpha = 18$ T, $F_\beta = 28$ T, $F_\gamma = 72$ T, and $F_\delta = 91$ T. These frequencies are very close to those obtained from the SdH oscillations, except for the notably larger F_α here [35]. From the Onsager relation $F = (\hbar/2\pi e)S_F$ [36], these low frequencies correspond to four small FSs. Moreover, there is an additional significant frequency at approximately 46 T in the FFT of the Nernst oscillations, and this frequency is less notable in the Seebeck and SdH oscillations [Fig. 4(c)]. This additional frequency is not a harmonic one of other frequencies but is roughly equal to the sum of F_α and F_β. In addition, it only occurs when the field is approximately higher than 3 T, as shown in Fig. 4(c). We attribute it to the magnetic breakdown across the orbits α and β. This quantum tunneling effect suggests their adjacent positions in the Brillouin zone [36].
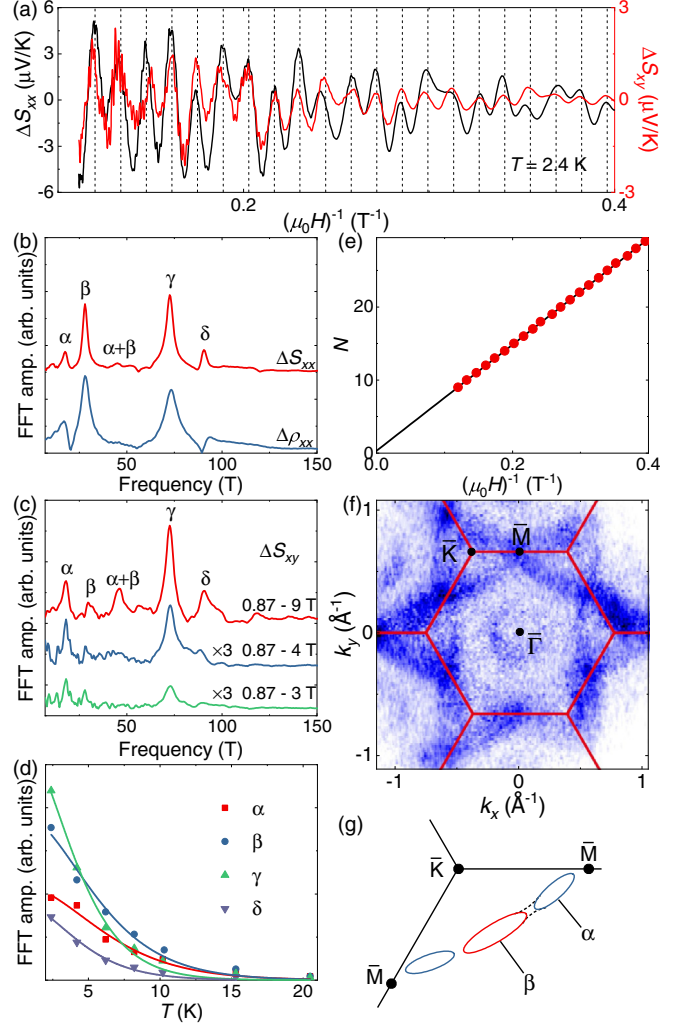
FIG. 4. (a) Oscillation parts of both S_{xx} and S_{xy} at 2.4 K. A primary frequency of $F_\gamma = 72$ T can be identified and the peaks are marked by dashes lines. (b) FFT spectrum of the Seebeck and SdH oscillations with the peaks are labeled. The highest peak γ corresponds to the primary frequency shown in (a). (c) FFT spectrum of the Nernst oscillations obtained from different magnetic ranges. A fifth peak with frequency close to $F_\alpha + F_\beta$ appears but is absent below 3 T. (d) Amplitudes of the four main peaks as a function of the temperature, with the solid lines representing the LK fitting. The effective masses obtained from ΔS_{xx} and ΔS_{xy} have very close values. (e) Index plot obtained from the primary oscillation of ΔS_{xx} shown in (a). (f) FS mapping measured by the ARPES at 33 K with the Brillouin zone and high-symmetry points superposed. (g) Possible sketch of FSs α and β, with a breakdown path marked by the dashed lines.

The Lifshitz-Kosevich (LK) theory describes the evolution of the quantum oscillations with the temperature and magnetic field [36], where the cyclotron effective mass and Dingle temperature are involved. For the oscillations in the thermoelectric coefficients, we fit the temperature dependence of the amplitudes of the oscillations using the following expression [37],

$$\frac{A}{T} \propto \frac{\lambda}{\sinh(\lambda)},$$
(3)

where A is the amplitude of ΔS_{xx} or ΔS_{xy}, $\lambda = 2\pi^2 k_B m^* T / e\hbar B$, and m^* is the cyclotron effective mass. For B, we use the average of the field range of oscillations, $1/B = 1/B_1 + 1/B_2$. Figure 4(d) shows the selected fitting results. Both ΔS_{xx} and ΔS_{xy} give consistent effective masses: $m_\alpha^* = 0.039m_0$, $m_\beta^* = 0.043m_0$, $m_\gamma^* = 0.058m_0$, and $m_\delta^* = 0.054m_0$. These light effective masses are close to the ones obtained from SdH oscillations [21].

Figure 4(e) shows the index plot of the primary oscillation shown in Fig. 4(a), and the $(\mu_0 H)^{-1}$ values correspond to the maxima of the ΔS_{xx} or ΔS_{xy}. The slope of the index plot gives a frequency of 72 T, which is consistent with the value of F_γ obtained by the FFT. Because S_{xx} and S_{xy} are the diagonal and off-diagonal terms of the tensor S, respectively, the maxima in ΔS_{xy} typically have a 1/4 phase shift relative to ΔS_{xx} [32]. However, there is no phase shift between ΔS_{xx} and ΔS_{xy} for the FS F_γ in CsV$_3$Sb$_5$, where a nontrivial Berry phase has been revealed by SdH oscillations [38]. The reason remains unclear and requires further investigations.

Understanding the band structure in the CDW state is one of the key topics of the AV$_3$Sb$_5$ compounds. Although density-functional-theory calculations can well explain the band structure observed in angle-resolved photoemission spectroscopy (ARPES) experiments [14], the four oscillation frequencies in the transport measurements remain poorly understood [35,38]. It suggests the delicate effect of the CDW modulation to the band structure. The electronic structure of undistorted CsV$_3$Sb$_5$ has three types of bands in the vicinity of the Fermi level: a parabolic electronic band near the $\overline{\Gamma}$ point, multiple Dirac bands around the $\overline{K}$ points, and saddle points or van Hove singularities at the $\overline{M}$ points [14,15], as shown in Fig. 4(f). The CDW transition in the AV$_3$Sb$_5$ system is commonly believed to be driven by the Peierls instability related to FS nesting [15]. The direct consequence of this instability is the gap opening on the FSs, which has been demonstrated by several experimental techniques [17–19,39–44]. Moreover, the CDW gap has a strong momentum dependence along the FSs of the Dirac bands [42,43]. The small effective masses obtained from our quantum oscillations indicate that these low-frequency oscillations originate from the Dirac bands. The FSs α and β may originate from a single band split by the CDW gap. Figure 4(g) shows a possible sketch of the FSs α and β, together with a breakdown path. The gap (ϵ_g) between them can be related to the threshold field of magnetic breakdown ($B^* \sim 3$ T) by $\hbar\omega_c \geqslant \epsilon_g^2/E_F$, where $\omega_c = eB^*/m^*$ [36]. With $E_F \sim 50$–80 meV given by the oscillations, the gap ϵ_g can be estimated less than $\sim$20 meV. This value is consistent with the CDW gap obtained from the spectroscopy experiments. This scenario can also be supported by the different F_α's between our work and Ref. [35] together with the three other consistent frequencies. In different samples, the strength of the CDW gap varies among them, leading to the different effects on the FS splitting.

The observed ANE reveals the TRSB in CsV$_3$Sb$_5$ again. Without local moments, the anomalous Nernst thermopower S_{xy}^A in this system can be as high as 4.4 μV/K at around 10 K. This large ANE is even competitive among the topological magnets [7,9]. From the quantum oscillations, we revealed two small FSs of the Dirac bands. The Dirac points, close to the Fermi level and gapped by the CDW modulation, can generate a large Berry curvature that contributes to the ANE. On the other hand, the strong correlation between the ANE and mobility suggests the extrinsic mechanisms also play important roles in the anomalous transport. The high conductivity of the crystals indicates the skew scattering is the most promising one [45]. To account for the TRSB in the CDW state of AV$_3$Sb$_5$ compounds, an unconventional chiral charge order was discovered [16,46], and an accompanying chiral flux phase was proposed [47,48]. For CsV$_3$Sb$_5$, the TRSB has been confirmed by multiple spectroscopic experiments [24,46], along with the AHE and our ANE [21,49]. Intriguingly, the AHE and the ANE appear below different temperatures, which are T_{CDW} and $\sim$30 K, respectively. It suggests their different sensitivities to the TRSB, and another phase transition may exist below T_{CDW}. Recently, muon spin rotation/relaxation (μSR) experiments revealed an additional TRSB phase transition far below T_{CDW} [24,50]. An x-ray diffraction experiment also revealed a CDW modulation transition below T_{CDW}, from the $2 \times 2 \times 4$ superstructure to the $2 \times 2 \times 2$ one at 60 K [51]. These results definitely indicate a second CDW phase with TRSB, which is responsible for the large ANE observed here.

In summary, we conducted a systematic investigation on the magnetothermoelectric effect of the kagome metal CsV$_3$Sb$_5$. We observe the large anomalous Nernst effect, and attribute it to both intrinsic and extrinsic mechanisms. The quantum oscillations of the thermoelectric coefficients reveal multiple Fermi surfaces and a magnetic breakdown effect across the two smallest ones. It indicates that the two smallest Fermi surfaces are split from a single Dirac band by the charge-density-wave gap. The anomalous Nernst component starts much below the charge-density-wave transition temperature, suggesting a second charge-density-wave phase with time-reversal symmetry breaking. Our results are significant for further study on the fine electronic structure, chiral flux phase, and novel superconductivity in the charge-density-wave state of kagome metal.

[1] K. Ohgushi, S. Murakami, and N. Nagaosa, Phys. Rev. B **62**, 6065(R) (2000).

[2] L. Balents, Nature (London) **464**, 199 (2010).

[3] L. Ye, M. Kang, J. Liu, F. Von Cube, C. R. Wicker, T. Suzuki, C. Jozwiak, A. Bostwick, E. Rotenberg, D. C. Bell *et al.*, Nature (London) **555**, 638 (2018).

[4] J.-X. Yin, W. Ma, T. A. Cochran, X. Xu, S. S. Zhang, H.-J. Tien, N. Shumiya, G. Cheng, K. Jiang, B. Lian *et al.*, Nature (London) **583**, 533 (2020).

[5] E. Liu, Y. Sun, N. Kumar, L. Muechler, A. Sun, L. Jiao, S. Y. Yang, D. Liu, A. Liang, Q. Xu *et al.*, Nat. Phys. **14**, 1125 (2018).

[6] Q. Wang, Y. Xu, R. Lou, Z. Liu, M. Li, Y. Huang, D. Shen, H. Weng, S. Wang, and H. Lei, Nat. Commun. **9**, 1 (2018).

[7] S. N. Guin, P. Vir, Y. Zhang, N. Kumar, S. J. Watzman, C. Fu, E. Liu, K. Manna, W. Schnelle, J. Gooth *et al.*, Adv. Mater. **31**, 1806622 (2019).

[8] S. Nakatsuji, N. Kiyohara, and T. Higo, Nature (London) **527**, 212 (2015).

[9] M. Ikhlas, T. Tomita, T. Koretsune, M.-T. Suzuki, D. Nishio-Hamane, R. Arita, Y. Otani, and S. Nakatsuji, Nat. Phys. **13**, 1085 (2017).

[10] A. K. Nayak, J. E. Fischer, Y. Sun, B. Yan, J. Karel, A. C. Komarek, C. Shekhar, N. Kumar, W. Schnelle, J. Kübler, C. Felser, and S. P. Parkin, Sci. Adv. **2**, e1501870 (2016).

[11] B. R. Ortiz, L. C. Gomes, J. R. Morey, M. Winiarski, M. Bordelon, J. S. Mangum, I. W. H. Oswald, J. A. Rodriguez-Rivera, J. R. Neilson, S. D. Wilson, E. Ertekin, T. M. McQueen, and E. S. Toberer, Phys. Rev. Materials **3**, 094407 (2019).

[12] B. R. Ortiz, P. M. Sarte, E. M. Kenney, M. J. Graf, S. M. L. Teicher, R. Seshadri, and S. D. Wilson, Phys. Rev. Materials **5**, 034801 (2021).

[13] Q. Yin, Z. Tu, C. Gong, Y. Fu, S. Yan, and H. Lei, Chin. Phys. Lett. **38**, 037403 (2021).

[14] B. R. Ortiz, S. M. L. Teicher, Y. Hu, J. L. Zuo, P. M. Sarte, E. C. Schueller, A. M. M. Abeykoon, M. J. Krogstad, S. Rosenkranz, R. Osborn, R. Seshadri, L. Balents, J. He, and S. D. Wilson, Phys. Rev. Lett. **125**, 247002 (2020).

[15] H. Tan, Y. Liu, Z. Wang, and B. Yan, Phys. Rev. Lett. **127**, 046401 (2021).

[16] Y.-X. Jiang, J.-X. Yin, M. M. Denner, N. Shumiya, B. R. Ortiz, G. Xu, Z. Guguchia, J. He, M. S. Hossain, X. Liu *et al.*, Nat. Mater. **20**, 1353 (2021).

[17] H. Chen, H. Yang, B. Hu, Z. Zhao, J. Yuan, Y. Xing, G. Qian, Z. Huang, G. Li, Y. Ye *et al.*, Nature (London) **599**, 222 (2021).

[18] H. Zhao, H. Li, B. R. Ortiz, S. M. Teicher, T. Park, M. Ye, Z. Wang, L. Balents, S. D. Wilson, and I. Zeljkovic, Nature (London) **599**, 216 (2021).

[19] Z. Liang, X. Hou, F. Zhang, W. Ma, P. Wu, Z. Zhang, F. Yu, J. J. Ying, K. Jiang, L. Shan, Z. Wang, and X. H. Chen, Phys. Rev. X **11**, 031026 (2021).

[20] S. Yang, Y. Wang, B. Ortiz, D. Liu, J. Gayles, E. Derunova, R. Gonzalez-Hernandez, L. Šmejkal, Y. Chen, S. Parkin *et al.*, Sci. Adv. **6**, eabb6003 (2020).

[21] F. H. Yu, T. Wu, Z. Y. Wang, B. Lei, W. Z. Zhuo, J. J. Ying, and X. H. Chen, Phys. Rev. B **104**, L041103 (2021).

[22] E. M. Kenney, B. R. Ortiz, C. Wang, S. D. Wilson, and M. J. Graf, J. Phys.: Condens. Matter **33**, 235801 (2021).

[23] C. Mielke III, D. Das, J.-X. Yin, H. Liu, R. Gupta, Y.-X. Jiang, M. Medarde, X. Wu, H. C. Lei, J. Chang, P. Dai, Q. Si, H. Miao, R. Thomale, T. Neupert, Y. Shi, R. Khasanov, M. Z. Hasan, H. Luetkens, and Z. Guguchia, Nature (London) **602**, 245 (2022).

[24] L. Yu, C. Wang, Y. Zhang, M. Sander, S. Ni, Z. Lu, S. Ma, Z. Wang, Z. Zhao, H. Chen *et al.*, arXiv:2107.10714.

[25] P. Hosur and X. Qi, C. R. Phys. **14**, 857 (2013).

[26] D. Xiao, M.-C. Chang, and Q. Niu, Rev. Mod. Phys. **82**, 1959 (2010).

[27] J. M. Ziman, *Electrons and Phonons* (Clarendon Press, Oxford, UK, 1960).

[28] T. Liang, J. Lin, Q. Gibson, T. Gao, M. Hirschberger, M. Liu, R. J. Cava, and N. P. Ong, Phys. Rev. Lett. **118**, 136601 (2017).

[29] J. L. Zhang, C. M. Wang, C. Y. Guo, X. D. Zhu, Y. Zhang, J. Y. Yang, Y. Q. Wang, Z. Qu, L. Pi, H. Z. Lu, and M. L. Tian, Phys. Rev. Lett. **123**, 196602 (2019).

[30] Z. Zhu, X. Lin, J. Liu, B. Fauqué, Q. Tao, C. Yang, Y. Shi, and K. Behnia, Phys. Rev. Lett. **114**, 176601 (2015).

[31] See Supplemental Material at http://link.aps.org/supplemental/10.1103/PhysRevB.105.L201109 for further details on the definitions of thermoelectric coefficients, the derivation of the two-band magneto-Seebeck expression, and the comparison of the Nernst signals of the two samples.

[32] T. Liang, Q. Gibson, J. Xiong, M. Hirschberger, S. P. Koduvayur, R. J. Cava, and N. P. Ong, Nat. Commun. **4**, 2696 (2013).

[33] S. J. Watzman, T. M. McCormick, C. Shekhar, S.-C. Wu, Y. Sun, A. Prakash, C. Felser, N. Trivedi, and J. P. Heremans, Phys. Rev. B **97**, 161404(R) (2018).

[34] Y. Gan, W. Xia, L. Zhang, K. Yang, X. Mi, A. Wang, Y. Chai, Y. Guo, X. Zhou, and M. He, Phys. Rev. B **104**, L180508 (2021).

[35] B. R. Ortiz, S. M. L. Teicher, L. Kautzsch, P. M. Sarte, N. Ratcliff, J. Harter, J. P. C. Ruff, R. Seshadri, and S. D. Wilson, Phys. Rev. X **11**, 041030 (2021).

[36] D. Shoenberg, *Magnetic Oscillations in Metals* (Cambridge University Press, Cambridge, UK, 1984).

[37] B. Fauqué, N. P. Butch, P. Syers, J. Paglione, S. Wiedmann, A. Collaudin, B. Grena, U. Zeitler, and K. Behnia, Phys. Rev. B **87**, 035133 (2013).

[38] Y. Fu, N. Zhao, Z. Chen, Q. Yin, Z. Tu, C. Gong, C. Xi, X. Zhu, Y. Sun, K. Liu, and H. Lei, Phys. Rev. Lett. **127**, 207002 (2021).

[39] X. Zhou, Y. Li, X. Fan, J. Hao, Y. Dai, Z. Wang, Y. Yao, and H.-H. Wen, Phys. Rev. B **104**, L041101 (2021).

[40] M. Kang, S. Fang, J.-K. Kim, B. R. Ortiz, S. H. Ryu, J. Kim, J. Yoo, G. Sangiovanni, D. D. Sante, B.-G. Park, C. Jozwiak, A. Bostwick, E. Rotenberg, E. Kaxiras, S. D. Wilson, J.-H. Park, and R. Comin, Nat. Phys. **18**, 301 (2022).

[41] K. Nakayama, Y. Li, T. Kato, M. Liu, Z. Wang, T. Takahashi, Y. Yao, and T. Sato, Phys. Rev. B **104**, L161112 (2021).

[42] Z. Wang, S. Ma, Y. Zhang, H. Yang, Z. Zhao, Y. Ou, Y. Zhu, S. Ni, Z. Lu, H. Chen *et al.*, arXiv:2104.05556.

[43] H. Luo, Q. Gao, H. Liu, Y. Gu, D. Wu, C. Yi, J. Jia, S. Wu, X. Luo, Y. Xu *et al.*, Nat. Commun. **13**, 273 (2022).

[44] Z. Liu, N. Zhao, Q. Yin, C. Gong, Z. Tu, M. Li, W. Song, Z. Liu, D. Shen, Y. Huang, K. Liu, H. Lei, and S. Wang, Phys. Rev. X **11**, 041010 (2021).

[45] N. Nagaosa, J. Sinova, S. Onoda, A. H. MacDonald, and N. P. Ong, Rev. Mod. Phys. **82**, 1539 (2010).

[46] Z. Wang, Y. X. Jiang, J. X. Yin, Y. Li, G. Y. Wang, H. L. Huang, S. Shao, J. Liu, P. Zhu, N. Shumiya, M. S. Hossain, H. Liu, Y. Shi, J. Duan, X. Li, G. Chang, P. Dai, Z. Ye, G. Xu, Y. Wang, H. Zheng, J. Jia, M. Z. Hasan, and Y. Yao, Phys. Rev. B **104**, 075148 (2021).

[47] X. Feng, K. Jiang, Z. Wang, and J. Hu, Sci. Bull. **66**, 1384 (2021).

[48] M. M. Denner, R. Thomale, and T. Neupert, Phys. Rev. Lett. **127**, 217601 (2021).

[49] G. Zheng, Z. Chen, C. Tan, M. Wang, X. Zhu, S. Albarakati, M. Algarni, J. Partridge, L. Farrar, J. Zhou *et al.*, arXiv:2109.12588.

[50] R. Khasanov, D. Das, R. Gupta, C. Mielke III, M. Elender, Q. Yin, Z. Tu, C. Gong, H. Lei, E. Ritz, R. M. Fernandes, T. Birol, Z. Guguchia, and H. Luetkens, arXiv:2203.12317.

[51] Q. Stahl, D. Chen, T. Ritschel, C. Shekhar, C. Felser, and J. Geck, arXiv:2112.02559.